BIOCHEMISTRY
including biophysical chemistry & molecular biology

ARTICLE

pubs.acs.org/biochemistry

Structural and Metal Binding Characterization of the C-Terminal Metallochaperone Domain of Membrane Fusion Protein SilB from *Cupriavidus metallidurans* CH34

Beate Bersch,[†] Kheiro-Mouna Derfoufi,[‡] Fabien De Angelis,[‡] Vanessa Auquier,[‡] Elisabeth Ngonlong Ekendé,[‡] Max Mergeay,[§] Jean-Marie Ruysschaert,[‡] and Guy Vandenbussche*[,‡]

[†]CNRS, Institut de Biologie Structurale Jean-Pierre Ebel, Grenoble, France, CEA, Institut de Biologie Structurale Jean-Pierre Ebel, Grenoble, France, and Université Grenoble 1, Institut de Biologie Structurale Jean-Pierre Ebel, Grenoble, France

[‡]Laboratory for the Structure and Function of Biological Membranes, Center for Structural Biology and Bioinformatics, Université Libre de Bruxelles, B-1050 Bruxelles, Belgium

[§]Molecular and Cellular Biology, Belgian Center for Nuclear Energy, SCK·CEN, B-2400 Mol, Belgium

Supporting Information

ABSTRACT: Detoxification of heavy metal ions in Proteobacteria is tightly controlled by various systems regulating their sequestration and transport. In *Cupriavidus metallidurans* CH34, a model organism for heavy metal resistance studies, the *sil* determinant is potentially involved in the efflux of silver and copper ions. Proteins SilA, SilB, and SilC form a resistance nodulation cell division (RND)-based transport system in which SilB is the periplasmic adaptor protein belonging to the membrane fusion protein (MFP) family. In addition to the four domains typical of known MFPs, SilB has a fifth additional C-terminal domain, called $SilB_{440-521}$, which is characterized here. Structure and backbone dynamics of $SilB_{440-521}$ have been investigated using nuclear magnetic resonance, and the residues of the metal site were identified from ^{15}N- and ^{13}C-edited HSQC spectra. The solution structure and additional metal binding experiments demonstrated that this C-terminal domain folds independently of the rest of the protein and has a conformation and a Ag^+ and Cu^+ binding specificity similar to those determined for CusF from *Escherichia coli*. The small protein CusF plays a role in metal trafficking in the periplasm. The similarity with CusF suggests a potential metallochaperone role for $SilB_{440-521}$ that is discussed in the context of simultaneous expression of different determinants involved in copper resistance in *C. metallidurans* CH34.

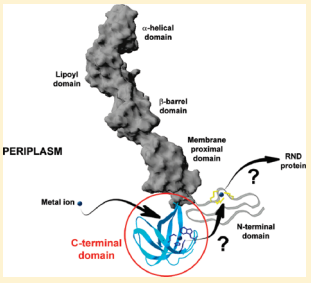

The membrane fusion protein (MFP) family comprises bacterial proteins with size, structural, and functional diversity (for a review, see ref 1). MFPs are working in conjunction with transporters that belong to the ATP-binding cassette (ABC), major facilitator (MF), and resistance nodulation cell division (RND) superfamilies and are present in both Gram-positive and Gram-negative bacteria (mainly Proteobacteria). While the ABC and MF superfamilies include uptake and efflux transporters, RND proteins catalyze only substrate efflux. In Proteobacteria, RND substrate/proton antiporters involved in resistance systems regulate the transport of a large range of cytotoxic compounds, including antibiotics and heavy metals.[2] On the basis of their respective substrates, these RND-driven systems are subdivided into the hydrophile/amphiphile efflux (HAE1) and heavy metal efflux (HME) families.[3] The tripartite resistance systems are formed by the association of an inner membrane RND protein, an outer membrane protein, a member of the outer membrane factor (OMF) family, and a periplasmic MFP,[4−6] also called periplasmic adaptor protein (PAP).[7] The RND and OMF proteins are present as stable homotrimers in cellular membranes, whereas the oligomeric state of the MFP component has not been unequivocally determined. The stoichiometry of the entire transporter was proposed to be RND_3-MFP_3-OMF_3, leading to a huge protein complex (>610000 Da) that spans the entire bacterial cell envelope.[8−10]

An increasing number of functions have been attributed to MFPs involved in RND-driven systems. MFPs play an important role in the recruitment of the OMF component and in the assembly of the tripartite protein complex by stabilizing weak RND−OMF interactions.[9,11−13] In addition, they facilitate substrate transport and are proposed to induce the fully open state of the OMF funnel.[10,14,15] Recent studies suggest that MFPs also participate actively in the efflux process. In particular, substrate binding has been demonstrated for two HME-type MFPs, CusB and ZneB,[16,17] and for HlyD, a MFP involved in type I export of hemolysin in *Escherichia coli*.[18] After binding, the substrate could be transferred by the MFP to the RND component.[17]

The three-dimensional structures of several MFPs belonging to RND-driven efflux systems have been determined.[17,19−22] These proteins have similar elongated structures characterized by four domains: the membrane proximal (MP), β-barrel, lipoyl,

Received: January 4, 2011
Revised: February 7, 2011
Published: February 07, 2011

and α-helical hairpin domains. The first MP domain structure has been determined recently for the HAE-type MFP MexA,[10] and afterward in the crystal structures of two HME-type MFPs, CusB and ZneB.[17,22]

We report here that besides these four canonical domains some MFPs possess an additional C-terminal domain. We have characterized this domain present in SilB, the MFP of the HME-RND-driven system SilABC from *Cupriavidus metallidurans* CH34. This metal-resistant β-Proteobacterium was isolated in Belgium from the sludge of a zinc decantation tank contaminated with high concentrations of several heavy metals[23,24] and is a model organism for the study of resistance to these toxic compounds and of the adaptation to extreme industrial or anthropogenic environments.[25,26] We have determined the three-dimensional solution structure of the SilB C-terminal domain by NMR, and we have confirmed Ag^+ and Cu^+ binding specificity of the experimentally identified metal coordination site. The metallochaperone role of this additional domain will be discussed.

EXPERIMENTAL PROCEDURES

Protein Expression and Purification. The coding sequence for the Gly_{440}−Pro_{521} domain of SilB (Uniprot/TrEMBL accession number Q58AF3) was amplified by PCR with Pfu polymerase (Fermentas) using genomic DNA from *C. metallidurans* CH34 as a template. The primers were designed to add an N-terminal six-His tag followed by a protease 3C cleavage site (forward primer, 5′-TATACATATGCACCATCATCATCATCATCTTGAAGTTCTTTTTCAAGGCCCAGAACATCGTGCAGTAGGG-3′; reverse primer, 5′-AATTAGATCTTCATGGCTTGGCTCCCGCGGTCTG-3′). After restriction enzyme digestion, the PCR product was ligated into the multiple-cloning site of a pET30b vector (Novagen) between the 5′ end *Nde*I and 3′ end *Bgl*II restriction sites. The construct was transformed into *E. coli* strain BL21(DE3) (Novagen) for protein production. For the sake of convenience, the resulting $SilB_{440-521}$ domain will be numbered from 1 to 82 in this work.

The transformed BL21(DE3) cells were grown in LB medium containing 30 μg/mL kanamycin at 37 °C with shaking at 180 rpm. To produce isotopically labeled protein, we cultured the transformed bacteria in M9 minimal mineral medium (pH 7.4), supplemented with 0.1 mM $MnCl_2$, 0.05 mM $FeCl_3$, 0.05 mM $ZnSO_4$, a vitamin solution, 30 mg/L kanamycin, and $^{15}NH_4Cl$ (1 g/L) (Cambridge Isotope Laboratories) and [$^{13}C_6$]glucose (2 g/L) (Euriso-Top) as the sole nitrogen and carbon sources, respectively.[27] In both media, the expression of the protein was induced when the cultures reached an absorbance of 0.8 at 600 nm by addition of 0.5 mM isopropyl β-D-1-thiogalactopyranoside (IPTG). After 4 h, the cells were harvested by centrifugation at 4 °C and kept at −80 °C.

The cell pellet corresponding to 1 L of culture was resuspended in 25 mL of 20 mM HEPES, 300 mM NaCl, and 10 mM imidazole (pH 7.8), with a protease inhibitor cocktail (Complete, Mini, EDTA-free tablets, Roche). The cells were lysed by being passed four times through an Emulsiflex (Avestin), and the cell suspension was centrifuged at 2000*g* for 10 min at 4 °C; the supernatant was further centrifuged at 10000*g* for 30 min at 4 °C. The supernatant was mixed with 2 mL of Ni-NTA resin (QIAGEN), and the suspension was incubated for 1 h at 4 °C under gentle agitation. The resin suspension was poured into a Poly-Prep column (Bio-Rad) and washed with 20 mL of 20 mM HEPES, 300 mM NaCl, and 10 mM imidazole (pH 8.0) and 12 mL of 20 mM HEPES, 300 mM NaCl, and 40 mM imidazole (pH 8.0). The protein was eluted with 2.5 mL of 20 mM HEPES, 300 mM NaCl, and 250 mM imidazole (pH 8.0). Prior to six-His tag cleavage, the buffer was exchanged for 5 mM HEPES (pH 7.0) on a PD-10 desalting column (GE Healthcare). The protein was incubated with a six-His-tagged protease 3C in 20 mM Tris-HCl, 150 mM NaCl, 2 mM EDTA, and 1 mM DTT (pH 7.0) at a 100:1 protein/enzyme mass ratio overnight at 4 °C. The cleaved six-His tag and the six-His-tagged protease 3C were trapped on a Ni-NTA column (QIAGEN), and the flow through containing the $SilB_{440-521}$ domain was collected. The protein was further purified by size exclusion chromatography (SEC) using a Superdex 200 10/300 GL analytical column connected to an Äktapurifier system (GE Healthcare). The protein was loaded onto the column pre-equilibrated with a selected buffer and eluted with the same buffer. This step also allowed us to transfer the protein in the different buffers used in this study. The column was calibrated with the Gel Filtration LWM Calibration Kit [aprotinin (6.5 kDa), ribonuclease A (13.7 kDa), carbonic anhydrase (29.0 kDa), ovalbumin (43.0 kDa), and conalbumin (75.0 kDa) (GE Healthcare)].

Finally, the purified $SilB_{440-521}$ domain was concentrated to 1 mM by ultrafiltration on an Amicon Ultra-4 5000 molecular weight cutoff centrifugal filter unit (Millipore). The protein concentration was determined by measuring the absorbance at 280 nm using a calculated molar extinction coefficient of 5500 M^{-1} cm^{-1}.

Mass Spectrometry. Spectra were recorded on an API hybrid quadrupole orthogonal time-of-flight mass spectrometer (Q-Tof Ultima, Waters), equipped with a nanoelectrospray source and operating in positive ion mode. Data were acquired using MassLynx version 4.0. For accurate molecular mass determination, protein was solubilized in a 50% acetonitrile/1% formic acid (v/v) mixture after being desalted on $ZipTipC_{18}$ (Millipore). Molecular masses were determined after MaxEnt1 deconvolution of the raw *m*/*z* data (Waters).

For the metal binding experiments, $SilB_{440-521}$ was solubilized in 10 mM ammonium acetate (pH 6.9). The protein was incubated at a final concentration of 5 μM in the presence of different heavy metals for 10 min at 22 °C. Parameters used for binding experiments were set to the following values: capillary voltage of 1600 V, cone voltage of 50 V, source block temperature of 100 °C, and pirani pressure of 2.2 mbar. Metal solutions were prepared using $AgNO_3$, $CdCl_2$, $CoCl_2$, $CuCl_2$, $NiCl_2$, $MnCl_2$, $Pb(CH_3COO)_2$, TlCl, and $ZnSO_4$ salts. Cu^+ was obtained by reduction of a Cu^{2+} solution in the presence of sodium ascorbate (pH 6.9) at a copper:reducer molar ratio of 1:4.

UV−Visible and Fluorescence Spectroscopy. $SilB_{440-521}$ was solubilized in 50 mM HEPES (pH 7.0) at a final concentration of 125 μM. The protein was titrated with 5 mM $AgNO_3$, and tryptophan absorption and emission spectra were recorded on an Agilent 8453 UV−visible spectrophotometer and an SLM Aminco 8000 fluorimeter, respectively. Emission spectra were recorded using an excitation wavelength of 280 nm. The titrations were conducted in 0.4 cm × 1 cm quartz cuvettes, and reaction solutions were mixed for 5 min before the spectra were recorded.

NMR Spectroscopy. NMR experiments were performed on Varian VNMRS 600 or 800 spectrometers equipped with triple-resonance (^1H, ^{13}C, and ^{15}N) cryoprobes and shielded z-gradients. All NMR experiments were conducted at 25 °C with a

sample concentration of 1.0 mM in 50 mM MES buffer (pH 6.0). Chemical shifts were referenced with respect to the H_2O signal at 4.77 ppm (pH 6.8, 25 °C) relative to DSS, using the ^{1}H:X frequency ratios of the zero point according to Markley et al.[28] All NMR spectra were processed and analyzed using NMRPipe[29] and NMRView.[30]

Sequential backbone resonance assignment of apo-SilB$_{440-521}$ was performed using the Batch strategy, which makes use of the fast data acquisition and analysis tools BEST,[31,32] ASCOM,[33] COBRA,[34] and HADAMAC,[35] and has been described in detail elsewhere (the HMR example in ref 36). Briefly, complete sequential ^{1}H, ^{15}N, and ^{13}CA resonance assignment was achieved from only four NMR experiments [BEST-^{1}H,^{15}N-HSQC, HADAMAC-2, BEST-HN(CO)CA, and BEST-intra-HNCA], acquired in less than 150 min of spectrometer time. Typically, all three-dimensional (3D) HNC experiments were conducted with the ^{15}N spectral width set to the ASCOM-derived optimal value of 784 Hz at a ^{15}N frequency of 60.8 MHz, and 19 complex data points were collected. For ^{13}CA frequency labeling, targeted regular sampling schemes were used as described previously.[34] Ten complex points were regularly collected at t_1 times from 0 to 3 ms, and 10 additional points were collected at t_1 times from 25 to 28 ms. ^{13}CB resonances were extracted from a BEST-HN(COCA)CB experiment[31] for which 30 complex points were collected in the ^{13}C dimension. Aliphatic carbon and proton side chain resonances were assigned from a ^{1}H,^{13}C-CT-HSQC experiment using intraresidual and sequential connectivity from two 3D ^{15}N- and ^{13}C-edited NOESY-HSQC experiments. The same experiments were also used for the extraction of ^{1}H−^{1}H distance restraints during structure calculation. Aromatic proton resonances were determined from a two-dimensional (2D) NOESY experiment conducted in D_2O. All NOE experiments were conducted using standard pulse sequences from the Varian Biopack with mixing times of 100 ms; 1024 × 150 × 40 and 1024 × 128 × 86 data points were acquired for the ^{15}N- and ^{13}C-edited NOESY experiments, respectively.

Ag^+- and Cu^+-SilB$_{440-521}$ NMR samples were prepared via addition of 1 molar equiv of $AgNO_3$ or $CuCl_2$ to the protein sample. Cu^+-SilB$_{440-521}$ was obtained in the presence of 10 molar equiv of sodium ascorbate. The ^{15}N chemical shifts of the histidine imidazole rings were determined from a modified SOFAST-HMQC experiment[37] optimized for the detection of $^2J_{NH}$ couplings. Selective proton pulses were centered at 7.4 ppm with a 2.5 ppm bandwidth, and the ^{15}N carrier frequency was set to 210 ppm. The ^{15}N spectral width was 6078 Hz at a ^{15}N frequency of 60.8 MHz. Backbone resonance assignment of Ag^+-SilB$_{440-521}$ was performed using a HADAMAC-2 experiment and 3D BEST-HNCOCA and BEST-HNCA experiments.[31] A 3D ^{13}C-edited NOESY-HSQC spectrum allowed assignment of the methionine $^{13}CH_3$ resonances for Ag^+-SilB$_{440-521}$.

Structure Calculation. Automatic peak picking and NOE assignment were performed using UNIO08[38,39] and the Cyana molecular dynamics algorithm.[39,40] Talos-derived[41] dihedral restraints together with long-range distance restraints, calculated from manually assigned NOEs involving aromatic side chain protons, were used as additional input data. Structures were refined using CNS[42] with the distance restraints obtained from UNIO08 together with the Talos-derived dihedral restraints. From an ensemble of 1000 structures, the 50 structures with the lowest total energy were selected and further refined in explicit water. The final structural ensemble is composed of the 20 structures with the lowest overall energy. The first structure of this ensemble is considered as the reference structure as it has the lowest experimental energy.

^{15}N Relaxation. R_1, $R_{1\rho}$, and heteronuclear $\{^1H\}-^{15}N$ NOE relaxation experiments were conducted at 600 MHz using standard pulse sequences.[43] Transverse relaxation rates were determined using $R_{1\rho}$-type rather than CPMG-type relaxation experiments to discard contributions from exchange between different conformations (R_{ex}) to total R_2 relaxation. Uniformly ^{15}N-labeled apo- and Ag^+-SilB$_{440-521}$ was used at a concentration of 1 mM. During the R_1 relaxation delays, cross-correlated relaxation was suppressed via application of a 550 μs cosine-modulated 180° squared pulse every 5 ms with an excitation maximum of 2 kHz from the carrier. The recycle delay was set to 3 s for the R_1 and $R_{1\rho}$ experiments, and the relaxation-caused magnetization decay was sampled at 10, 30, 60, 120, 180, 240, 300, 400, 600, 900, and 1100 ms for longitudinal and at 10, 30, 50, 70, 90, 130, 170, 210, 280, and 400 ms for transverse relaxation. For the heteronuclear $\{^1H\}-^{15}N$ NOE, a 1.7 kHz WALTZ16 decoupling scheme centered at the amide proton frequencies was applied to saturate the amide proton signals. The saturation and recycle delays were set to 3 and 5 s, respectively.

Peak intensities were measured with NMRView, and relaxation rates were extracted using the Curvefit program (http://biochemistry.hs.columbia.edu/labs/palmer/software/curvefit.html) assuming a two-parameter single exponential with a Monte Carlo simulation for error estimation, taking into account twice the root-mean-square (rms) noise of the spectra. Residues with overlapping resonances were excluded from the analysis. Transverse relaxation rates were calculated from the $R_{1\rho}$ rate constants using the relation

$$R_{1\rho} = \cos^2(\theta)R_1 + \sin^2(\theta)R_2$$

with

$$\theta = \tan^{-1}(\gamma_N B_1/2\pi\Delta\nu)$$

$\{^1H\}-^{15}N$ steady-state NOE values were obtained from the ratio of cross-peak intensities from the spectra obtained with and without proton saturation. Apo-SilB$_{440-521}$ mobility was further analyzed with Tensor2,[44] which uses the model-free approach of Lipari and Szabo.[45,46] The extracted relaxation rates and the heteronuclear NOE were used as input data, assuming an error of 5%, and the first structure of the structural ensemble was taken as a reference. ^{15}N R_1 and R_2 relaxation rates of residues with heteronuclear NOEs of >0.72 were fit to isotropic and anisotropic models for overall rotation, with extensive Monte Carlo simulations to test the relevance of the improvement available from the more complex fit using F testing. This showed that an axially anisotropic model is required to properly fit the data. Full model-free analysis was then performed on the ensemble of residues for which a complete data set was available. Relaxation data for all but one residue (Thr_{34}) could be fitted to one of the following dynamic models of spectral density function: (1) S^2, (2) S^2 and τ_i, and (3) S^2 and R_{ex}. The appropriate models were chosen using an iterative fitting procedure, and the selection was based on 300 Monte Carlo simulations to provide probability statistics and error analysis.

RESULTS

Alignment of MFPs from *C. metallidurans* CH34. The sequences of 10 MFPs belonging to predicted HME-RND-driven

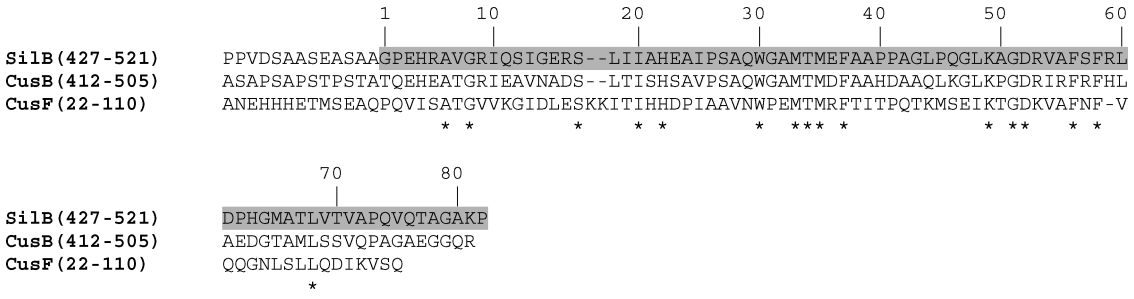

Figure 1. Sequence alignment of SilB and CusB C-terminal domains from *C. metallidurans* CH34 and CusF from *E. coli* generated by ClustalX. Residues marked with stars are conserved in the three proteins. The $SilB_{440-521}$ domain is highlighted in gray and numbered from 1 to 82.

systems from *C. metallidurans* CH34 were aligned using Expresso (3D-Coffee)[47] (Figure S1 of the Supporting Information). The multiple-sequence alignment shows that three proteins, CzcB, SilB, and CusB, contain additional domains in comparison with the other MFPs. As previously described, CzcB contains an N-terminal domain that includes two homologous histidine-rich segments.[5] These motifs were proposed to form a zinc-binding site, but they are not essential for cation detoxification by the CzcCBA system.[48] More interesting is the presence of additional N- and C-terminal extensions in SilB and CusB. These two proteins are part of the SilABC and CusCBA systems, respectively, both of which are potentially involved in the resistance to silver and copper in *C. metallidurans* CH34.[49,50] It is not surprising to find a similar domain composition in both proteins as *silB* and *cusB* genes are paralogs and the corresponding proteins are 51% identical in sequence. The ~100-residue C-terminal domains observed in SilB and CusB have sequences similar to that of CusF, a small periplasmic protein that is the fourth component of the HME-RND-type CusCFBA system that confers copper and silver resistance in *E. coli* (Figure 1). CusF is not an essential component of the Cus system but is required for optimal function.[51] The particularity of SilB and CusB from *C. metallidurans* CH34 resides in the fact that this CusF homologous domain is fused to the MFP C-terminus forming a single protein chain.

In addition, the structural sequence alignment generated using 3D-Coffee reveals in SilB and CusB a region upstream of the residues belonging to the N-terminal portion of the MP domain (Figure S1 of the Supporting Information, residues K_{59}—E_{93} in SilB) that seems specific to these proteins involved in the transport of monovalent cations. This domain, highly conserved within CusB- and SilB-like proteins (data not shown), contains the three conserved methionines that were identified as Ag^+ and Cu^+ ligands in *E. coli* CusB[16] and may form an additional structural domain.

Here, we will characterize the C-terminal domain from *C. metallidurans* SilB, $SilB_{440-521}$, as a first step toward an improved understanding of metal ion transport processes in these specific tripartite HME-RND-driven transporters.

Production and Purification of $SilB_{440-521}$. The domain corresponding to residues Gly_{440}—Pro_{521} in the unprocessed protein SilB (Figure 1) was overexpressed in *E. coli* strain BL21(DE3) and purified by immobilized metal ion affinity chromatography (IMAC) followed by size exclusion chromatography (SEC). The quality of the preparation and the integrity of the recombinant protein were checked by gel electrophoresis and mass spectrometry, respectively (Figure S2 of the Supporting Information). For NMR purposes, the protein was isotopically labeled with ^{15}N or with ^{15}N and ^{13}C. More than 98% of the total isotope enrichment was obtained as confirmed by mass spectrometry. Regardless of the buffer used (50 mM MES for pH 6.0, 5 mM HEPES for pH 7.0, or 10 mM ammonium acetate for pH 6.9), the protein was eluted as a monomer on a Superdex 75 column (data not shown).

Metal Binding Specificity. The metal binding specificity of $SilB_{440-521}$ was monitored by mass spectrometry. The protein purification buffer was exchanged by SEC for a nondenaturing volatile buffer compatible with the ESI-MS approach [10 mM ammonium acetate (pH 6.9)]. Mass spectra were recorded after incubation of the protein in the presence of different metal ions (Ag^+, Cd^{2+}, Co^{2+}, Cu^+, Cu^{2+}, Mn^{2+}, Ni^{2+}, Pb^{2+}, Tl^+, or Zn^{2+}) under conditions preserving noncovalent metal ion—protein interaction. Addition of 1 molar equiv of Ag^+ or Cu^+ induced a shift of the protein peaks to higher m/z values corresponding to the binding of one metal ion per protein (Figure 2). No metal—protein complex was observed in the presence of the other metal ions (Figure 2), even at a cation: protein molar ratio of 1:4 (data not shown). Our data strongly suggest Ag^+ and Cu^+ binding specificity of the $SilB_{440-521}$ domain. The coordination of copper is dependent on the oxidation state of the metal ion as no binding was observed in the presence of Cu^{2+}. Because of the high propensity of Cu^+ to be oxidized in Cu^{2+}, we have confirmed by mass spectrometry that once bound, the ion remains in the cuprous state.[52] A high-resolution mass spectrum of $SilB_{440-521}$ in the presence of 1 molar equiv of Cu^+ was recorded to visualize the isotopic distribution. The most abundant ion observed corresponds to the protein—copper complex bearing six positive charges. These six positive charges can result from two situations: either $SilB_{440-521}$ with Cu^+ and $5H^+$ or $SilB_{440-521}$ with Cu^{2+} and $4H^+$; the corresponding theoretical m/z values for the monoisotopic mass (i.e., the calculated mass of a compound containing the principal isotope of each atom making up the original molecule) are 1433.9018 and 1433.7339 Th, respectively. The experimental 1433.90 Th value observed for the monoisotopic peak of the 6+ isotopic cluster confirmed the presence of a cuprous ion bound to the $SilB_{440-521}$ domain.

Characterization of the Metal Coordination Site. Figure S3 of the Supporting Information shows the comparison of ^1H,^{15}N-HSQC spectra for apo and metal-bound $SilB_{440-521}$. The variation of the backbone chemical shifts for residues His_{22}, Trp_{30}, Met_{33}, and Met_{35}, as well as for two nearby residues (Thr_{34} and Glu_{36}), suggests that these residues could play a large part in the metal-binding site of $SilB_{440-521}$. This was further confirmed by a direct identification of metal-binding residues. It has previously been shown that histidine and methionine residues forming a Cu^+ site can unambiguously be identified from

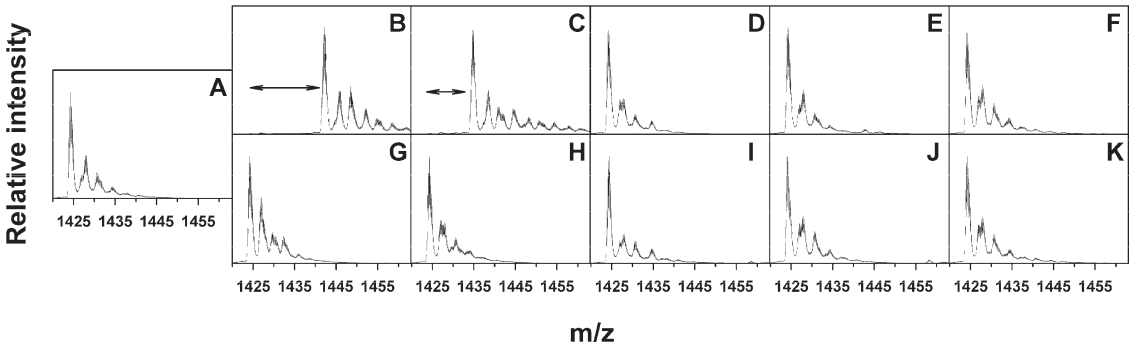

Figure 2. ESI mass spectra for the 6+ charge state of 5 μM $SilB_{440-521}$ in 10 mM ammonium acetate (pH 6.9): (A) apo form and forms in the presence of 1 molar equiv of (B) Ag^{+}, (C) Cu^{+}, (D) Cu^{2+}, (E) Cd^{2+}, (F) Co^{2+}, (G) Mn^{2+}, (H) Ni^{2+}, (I) Pb^{2+}, (J) Tl^{+}, or (K) Zn^{2+}. The arrows in panels B and C indicate the mass shift resulting from the binding of one molecule of Ag^{+} and Cu^{+}, respectively.

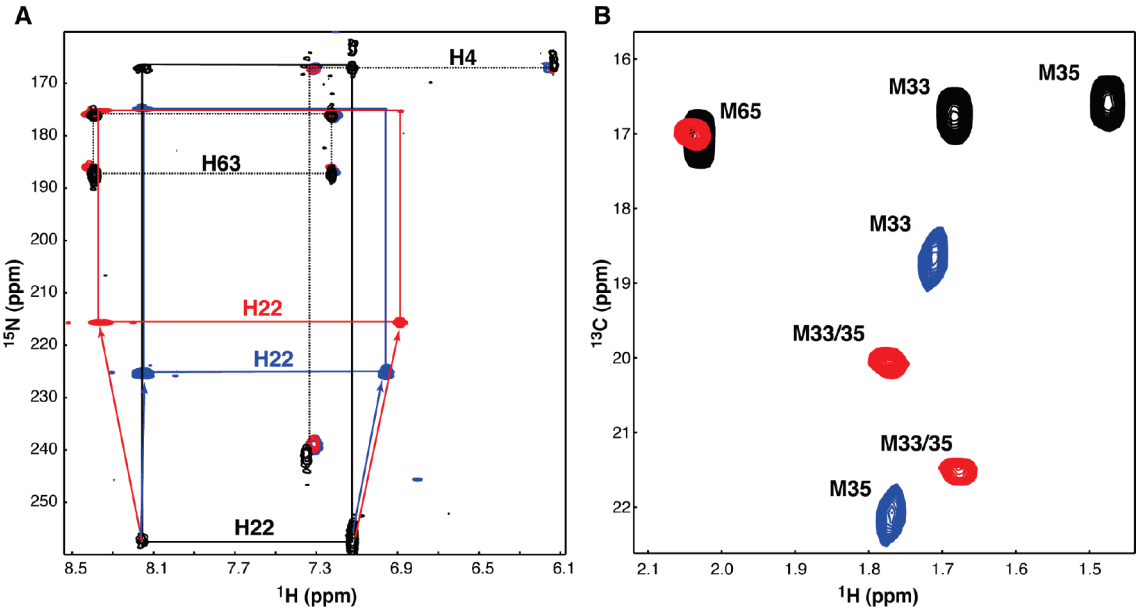

Figure 3. Identification of metal ligands from NMR. HSQC spectra of apo-$SilB_{440-521}$ (black), Ag^{+}-$SilB_{440-521}$ (blue), and Cu^{+}-$SilB_{440-521}$ (red). (A) $^{1}H,^{15}N$-HSQC spectrum optimized for the detection of $^{2}J_{HN}$ couplings displaying the $^{1}H-^{15}N$ correlations within the histidine imidazole ring. Spin systems are linked by dotted lines for His_4 and His_{63} and by solid lines for His_{22}, which is involved in Ag^{+} and Cu^{+} binding. The chemical shift variation of Nε2 upon metal binding is indicated by the arrows. (B) Section of a $^{1}H,^{13}C$-HSQC spectrum displaying the methionine methyl $^{1}H-^{13}C$ correlations. Metal binding to methionine Sδ induces a downfield shift of the Cε resonance. No sequence specific side chain assignment was attempted for Cu^{+}-$SilB_{440-521}$. In Ag^{+}-$SilB_{440-521}$, the Met_{65} $^{1}H-^{13}C\varepsilon$ peak is broadened to below the detection limit.

NMR chemical shift variations of the imidazole nitrogen and the methionine methyl carbon resonances.[53−55] Figure 3 shows the corresponding $^{1}H,^{15}N$ and $^{1}H,^{13}C$ spectra that clearly demonstrate that His_{22}, Met_{33}, and Met_{35} are involved in Ag^{+} and Cu^{+} binding. The chemical shifts of Met_{65}, His_{63}, and His_4 do not change upon metal interaction except for the Met_{65} $^{1}H-^{13}C\varepsilon$ peak that could not be detected in the case of Ag^{+}-$SilB_{440-521}$, presumably because of severe line broadening.

The involvement of Trp_{30} in metal ion binding was also investigated by monitoring the interaction of Ag^{+} with the tryptophan aromatic ring by UV and fluorescence spectroscopy. The $SilB_{440-521}$ domain contains a single tryptophan, Trp_{30}, and no tyrosine residue. Titration of $SilB_{440-521}$ with Ag^{+} ions induced a quenching of the Trp_{30} emission at 343 nm (Figure 4A) and a red shift of the Trp_{30} absorption at 280 nm (Figure 4B). For both measurements, no further spectral modifications were observed when a 1:1 protein:metal ion molar equivalent ratio was reached (see the insets of Figure 4A,B). No modification of the spectral features of Trp_{30} was detected upon titration of the protein with Cd^{2+} ions, a metal that does not interact with $SilB_{440-521}$ (data not shown).

Three-Dimensional Structure of Apo-$SilB_{440-521}$ Determined by NMR. Nearly complete ^{1}H, ^{13}C, and ^{15}N resonance assignment could be obtained from a series of 2D and 3D NMR experiments as described in Experimental Procedures. The assigned $^{1}H,^{15}N$-HSQC spectrum of apo-$SilB_{440-521}$ is shown in Figure S4 of the Supporting Information; 1597 unambiguous distance constraints were generated by UNIO08[38,39] from two isotope-edited NOESY spectra and were used as input for structure calculation together with 188 manually assigned distance constraints and 92 TALOS-derived dihedral angle constraints. The final structural ensemble was calculated with an explicit water refinement using CNS.[42] This ensemble comprises 20 structures that are shown superimposed in Figure 5A.

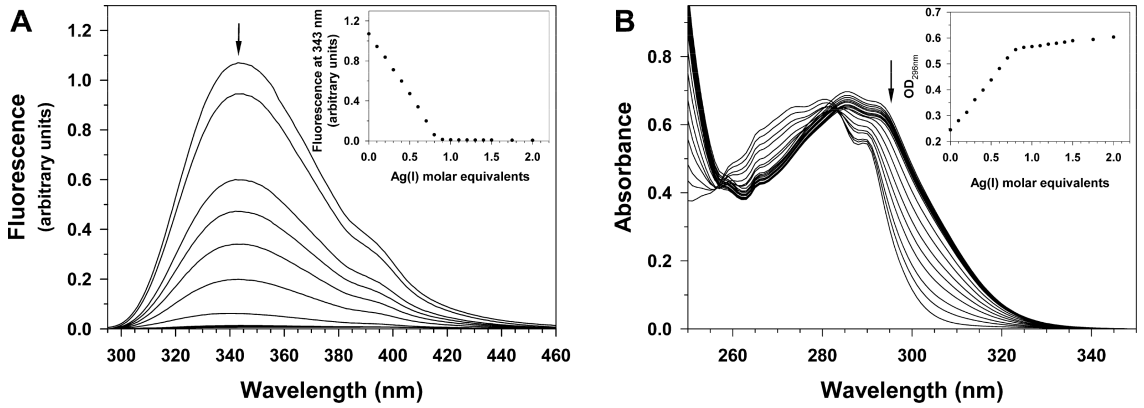

Figure 4. (A) Quenching of the Trp_{30} fluorescence emission upon titration of $SilB_{440-521}$ (125 μM) in 50 mM HEPES buffer (pH 7.0) with 5 mM $AgNO_3$. The inset represents the evolution of the emission at 343 nm (arrow) as a function of the number of silver molar equivalents. (B) Modification of the Trp_{30} UV spectrum upon titration of $SilB_{440-521}$ (125 μM) in 50 mM HEPES buffer (pH 7.0) with 5 mM $AgNO_3$. The inset represents the evolution of A_{296} (arrow) as a function of the number of silver molar equivalents.

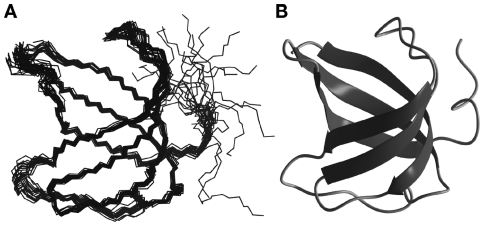

Figure 5. Solution structure of apo-$SilB_{440-521}$. (A) Structural ensemble comprising 20 selected conformers that are shown superimposed with respect to the mean conformation. (B) Ribbon diagram of the representative solution structure.

Structural statistics are listed in Table 1. The structure is well-defined with a backbone root-mean-square deviation (rmsd) of 0.5 Å calculated for residues 3−75. $SilB_{440-521}$ adopts an OB-fold[56] consisting of a small β-barrel formed by five β-strands [residues 3−12, 17−22, 33−38, 53−61, and 65−73 (Figure 5B)].

Comparison of Apo- and Ag^+-$SilB_{440-521}$. Comparison of chemical shifts reports on local effects of metal binding as they strongly depend on the electronic environment of the observed nuclei. We have shown above that side chain chemical shifts allow identification of the metal-binding residues. Backbone chemical shift variation on the other hand may indicate conformational changes that are induced by the protein−metal interaction. In Figure S5 of the Supporting Information, we show the weighted chemical shift differences $\{[\Delta HN^2 + \Delta N^2 \times (\gamma_N/\gamma_H)^2]^{1/2}\}$ observed on amide proton and nitrogen frequencies between apo- and Ag^+-$SilB_{440-521}$. To this end, a complete backbone assignment of Ag^+-$SilB_{440-521}$ has been obtained as described in Experimental Procedures. Changes of more than 0.2 ppm were considered significant and are shown plotted on the backbone of $SilB_{440-521}$ in the inset of Figure S5 of the Supporting Information. It can be seen that residues undergoing significant changes are located in the vicinity to the formerly identified residues in the metal site, suggesting a local perturbation due to metal binding.

We also investigated protein backbone mobility of apo- and Ag^+-$SilB_{440-521}$ by measuring ^{15}N spin relaxation rates at 600 MHz and 25 °C. Longitudinal (R_1) and transverse relaxation ($R_{1\rho}$) rates could be determined for 63 and 57 residues in apo- and Ag^+-$SilB_{440-521}$, respectively. Panels A and B of Figure 6 show the comparison of the measured relaxation rates for the two protein forms. It can be seen that R_1 rates are virtually the same for the metal-bound and apo forms of $SilB_{440-521}$, as are the $R_{1\rho}$-derived transverse relaxation rates for residues in β-strands 1, 4, and 5. From these data, one can conclude that the overall rotational tumbling of the protein is not modified because of metal binding and that backbone mobility on the fast time

Table 1. Statistics for the Final Structural Ensemble (20 structures)

coordinate precision (residues 3−75)	
rmsd for C′, Cα, N (Å)	0.5 ± 0.09
rmsd for heavy atoms (Å)	0.88 ± 0.09
structural statistics	
energy (kcal/mol)	
bond	22.3677 ± 1.87631
angle	80.4879 ± 6.16987
improper	207.527 ± 19.5414
dihedral	374.7 ± 5.46742
van der Waals	−663.92 ± 8.06717
electrostatics	−2854.39 ± 35.2116
violation energy	42.57 ± 7.3014
total	−2579.47 ± 36.0313
rmsd from idealized geometry	
bond lengths (Å)	0.0043 ± 0.0002
angles (deg)	0.487 ± 0.018
impropers (deg)	1.468 ± 0.070
Ramachandran statistics (PROCHECK) (residues 3−75)	
residues in most favored regions (%)	81
residues in additional allowed regions (%)	17.5
residues in generously allowed regions (%)	0.8
residues in disallowed regions (%)	0.7

Experimental Statistics	no. of restraints	rmsd
distance restraints (Å)	1597	0.022 ± 0.001
dihedral restraints (deg)	92	0.66 ± 0.12

dx.doi.org/10.1021/bi200005k |*Biochemistry* 2011, 50, 2194–2204

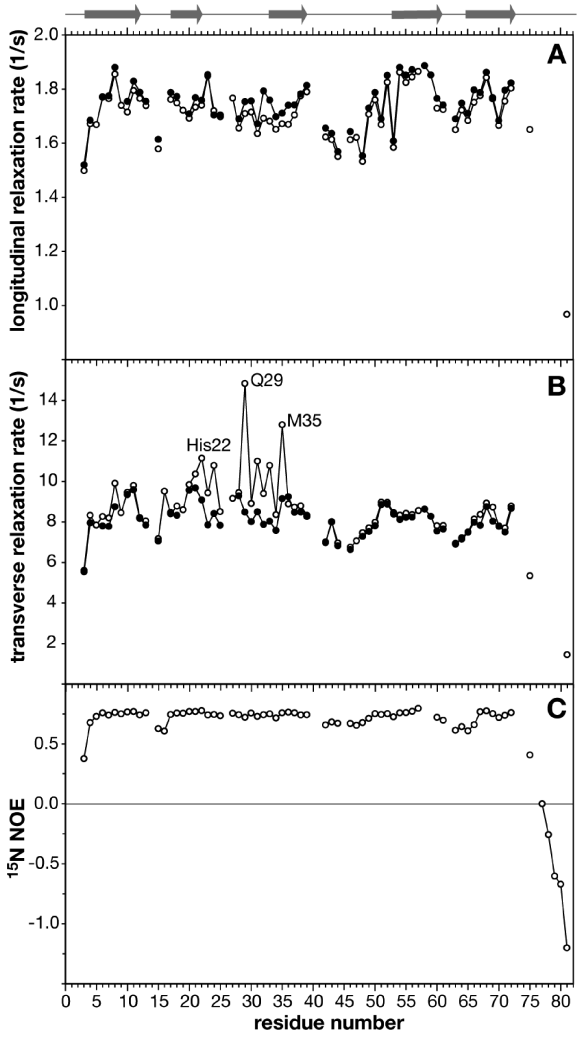

Figure 6. ^{15}N relaxation of apo- and Ag^{+}-$SilB_{440-521}$. Longitudinal (A) and transverse (B) ^{15}N relaxation rates as well as the $\{^{1}H\}-^{15}N$ NOEs (C) are plotted as a function of the protein sequence. Empty and filled circles correspond to data for apo-$SilB_{440-521}$ and Ag^{+}-$SilB_{440-521}$, respectively. Transverse relaxation rates ($R_{1\rho}$) were calculated considering the ^{15}N resonance offset with respect to the spin lock field as described in Experimental Procedures. The position of the β-sheets within the protein is indicated.

scale, sampled by R_1, is the same for both forms. Significant differences are observed in the profile of the transverse relaxation rates (Figure 6B). Indeed, residues His_{22}, Ala_{24}, Gln_{29}, Ala_{31}, Met_{33}, and Met_{35} show increased transverse relaxation rates in the apo form of $SilB_{440-521}$. Whereas longitudinal relaxation samples backbone mobility on the pico- to nanosecond time scale, transverse relaxation also senses slower protein motions on the micro- to millisecond time scale. The comparison of the values obtained for the two forms suggests that the metal-binding loop between residues 20 and 37 undergoes slow motions in the apo state that are abolished once the metal is bound. Interestingly, there is no strong correlation between the transverse relaxation rates and the observed chemical shift differences between apo- and Ag^{+}-SilB. This suggests that the apoprotein does not simply exchange with a conformation that is close to the metal-bound state. A complete mobility analysis of apo-$SilB_{440-521}$ using a Lipari−Szabo-type approach provided by Tensor2[44] was also performed. To this end, $\{^{1}H\}-^{15}N$ NOEs were also measured for the apoprotein (see Figure 6C). The overall rotational motion was characterized using R_1- and $R_{1\rho}$-derived R_2 relaxation rates measured for residues with an $\{^{1}H\}-^{15}N$ NOE of >0.72 but excluding residues 23−32 of the metal-binding loop. The data could be fitted assuming isotropic reorientation with a τ_c of 6.28 ± 0.04 ns. However, the fit significantly improved when an axially isotropic rotational diffusion tensor was used with the following values: $D_{\|} = (3.19 \pm 0.1) \times 10^{-7}\ s^{-1}$, and $D_{\perp} = (2.4 \pm 0.04) \times 10^{-7}\ s^{-1}$. No further improvement could be obtained using a fully anisotropic tensor. The results of the mobility analysis, generalized order parameters, S^2, internal correlation times, τ_i, and conformational exchange rates, R_{ex}, are shown in Figure S6 of the Supporting Information. It can be seen that apo-$SilB_{440-521}$ globally is a rigid molecule with order parameters of >0.8 for most residues, indicating restrained internal motion on the pico- to nanosecond time scale. Slightly lower order parameters were observed for residues in the N-terminus and in surface loops between β-strands 3 and 4 and between β-strands 4 and 5 (compare the inset to Figure S6C of the Supporting Information). The results of the mobility analysis indicate fast motions with an internal correlation time of ∼70 ps (Figure S6B of the Supporting Information). As already suggested from the comparison of the relaxation rates, residues belonging to the metal-binding loop are subjected to slow motions. This translates into the conformational exchange terms shown in Figure S6C of the Supporting Information. It can be seen that the presence of such slow motions is limited to the metal-binding loop. The highest exchange rates were detected for Gln_{29} at the top of the loop and Met_{35}, one of the Cu^{+} ligands.

DISCUSSION

The cellular copper concentration is controlled in bacteria by numerous pathways, such as enzymatic transformation, sequestration, and more importantly active transport. Under physiological conditions, this essential trace element exists in two oxidation states, Cu^{2+} and Cu^{+}, and several proteins involved in Cu^{+} transport also interact with Ag^{+}, because of the similarity of the electronic structure of these two ions. An example is the well-characterized copper- and silver-transporting RND-driven system CusCFBA from *E. coli*.[51] In addition to the canonical tripartite architecture, the CusCFBA complex in particular contains a fourth protein, CusF. Among the different functions proposed for this small periplasmic protein, CusF could play the role of a metallochaperone that binds metal ions in the periplasm and transfers them to the CusCBA efflux machinery.[57] CusF homologues are found in other bacterial genomes not only as a single protein but also fused with the C-termini of some MFPs.

To characterize the properties of these CusF homologues covalently linked to the MFP polypeptidic chain, we have studied SilB, the periplasmic component of the SilABC system. This protein complex is one of the two RND-based efflux systems potentially involved in silver and copper resistance in *C. metallidurans* CH34 and the only one to be encoded by plasmid pMOL30, which is specialized in the response and/or resistance to very high heavy metal concentrations as found in metallurgical tailings.[26] We have expressed and purified the SilB C-terminal subdomain, $SilB_{440-521}$, and we have shown that this domain has metal coordination site and metal binding specificity similar to that of CusF from *E. coli*. Our data demonstrated that this

Figure 7. Comparison of the backbone conformation and metal site of apo-SilB$_{440-521}$ and *E. coli* apo-CusF (Protein Data Bank entry 1ZEQ). SilB$_{440-521}$ is colored red and CusF green. The side chains of residues in the metal site are shown with the sulfur atoms of the two methionines colored yellow.

coordination site seems to have substrate specificity limited to Ag^+ and Cu^+ and not to monovalent ions in general as no binding of Tl^+, for example, was observed for SilB$_{440-521}$. We also determined the three-dimensional structure of SilB$_{440-521}$ by solution NMR showing that both proteins share the same fold composed of a small β-barrel formed by five β-strands. This conformation is characteristic of proteins belonging to the OB-fold (oligonucleotide/oligosaccharide binding) family,[56] and CusF is, until now, the only known metal-binding protein adopting this fold. Figure 7 shows the comparison between the backbone coordinates of the apo-SilB$_{440-521}$ solution structure and the crystal structure of *E. coli* apo-CusF (Protein Data Bank entry 1ZEQ[58]). The backbone atoms of these structures superpose with an rmsd of 1.17 Å (calculated over 264 atoms using DeepView[59]). From Figure 7, one can see that in the apo forms of the two proteins, the amino acids involved in metal binding are remarkably well superimposed, indicating the strict conservation of the metal site. In addition, the structural differences between the apo and metal-bound forms of SilB$_{440-521}$ as monitored by the chemical shift differences shown in Figure S5 of the Supporting Information are strictly comparable to what has been seen for *E. coli* CusF from the comparison of NMR data[58] and the crystal structures of apo-, Cu^+-, and Ag^+-CusF.[60,61] In this study, we also present a comparative study of the backbone dynamics of the two forms of SilB$_{440-521}$ that reveals the contribution of slow motions to ^{15}N relaxation in the loop that forms the metal-binding site. Slow motions in metal-binding loops have already been observed in Atx1-like metallochaperones.[62−64] In these proteins, correlation peaks of residues close to the two cysteines involved in the Cu^+ site frequently appear to be broadened in ^{1}H,^{15}N-HSQC spectra of the apoproteins. As in the case of SilB$_{440-521}$, the metal loop becomes structured once the metal is bound. However, a different behavior has recently been found in the case of CopK, a small periplasmic copper protein from *C. metallidurans* CH34 encoded, like SilB, by plasmid pMOL30.[54,55,65] In CopK, the apo form appeared to be more structured than the metal-bound protein. This was, however, not limited to residues directly involved in the metal site as metal interaction induced partial dissociation of a β-sheet.[55]

This C-terminally fused CusF-like domain of SilB seems to be totally independent of the rest of the protein in terms of structure and function. Indeed, our data show that the isolated SilB$_{440-521}$ domain is able to adopt a correct fold and presents a biological activity, i.e., the specific binding of silver and copper ions, and provide experimental evidence that SilB from *C. metallidurans* CH34 is to be considered as the fusion of two proteins homologous to CusB and CusF from *E. coli*, respectively. Consequently, from a structural point of view, SilB-like proteins containing the C-terminal CusF-like extension deviate from the classical four-domain structure observed in MexA, CusB, and ZneB[10,17,22] as they present a fifth ordered domain.

In a manner independent of the presence of the C-terminally fused CusF-like domain, MFPs presumably involved in the transport of monovalent copper and silver ions, i.e., CusB- and SilB-like proteins, contain three conserved methionine residues in their N-terminal region reported to be essential for the specific binding of Ag^+ and Cu^+ in CusB from *E. coli*.[51] A Blast alignment of *C. metallidurans* CH34 SilB against the UniRef50 database reveals that this N-terminal region formed of approximately 35 residues is highly conserved. This region was not identified in the electron density maps of *E. coli* CusB crystals and is proposed to be disordered.[22] However, the possibility that this domain could adopt an ordered structure upon binding of silver or copper ions cannot be excluded. As crystals of the CusB metal-bound form were obtained by soaking the crystals in metal solutions and not by adding the metal ions during the crystallization steps, such a structural reorganization may have been impeded by molecular contacts in the crystal lattice.

What could be the role of the CusF-like domain in *C. metallidurans* CH34 SilB? In *E. coli*, it was demonstrated that CusF and CusB interact in the presence of metal ions, triggering metal ion transfer between them.[66] This transfer is made possible by the similarity in metal ion affinity for both proteins.[16,67] As described above, *C. metallidurans* CH34 SilB can be considered as a fusion between a CusB- and CusF-like protein and therefore contains two coordination sites potentially involved in an intramolecular metal ion transfer. As the structure of *E. coli* CusB has shown that the N- and C-termini are very likely in the proximity of each other,[22] such a transfer would not necessarily involve a major, structural rearrangement. Indeed, flexibility in the linker regions between the different protein domains was described in ZneB, CusB, MexA, and AcrA[10,17,21,22,68] and could further promote the interaction between the two metal-binding sites in SilB. In this case, the SilB$_{440-521}$ domain may have a role in carrying metal ions from the periplasm to the N-terminal coordination site of SilB, before their possible transfer to the RND transporter SilA. We have proposed a mechanism of substrate binding by the MFP and release to the RND protein on the basis of a zinc-triggered structural change occurring in ZneB, a MFP from a *C. metallidurans* CH34 zinc resistance system.[17] It is unlikely that the transfer of the metal ion could proceed from the MFP to the OMF component as the metal ion-binding site in the former is opposite to the MFP−OMF interaction domain.

A fusion between the CusB- and CusF-like proteins to a single protein chain may confer significant advantages in a situation in which different metal transfer mechanisms are simultaneously

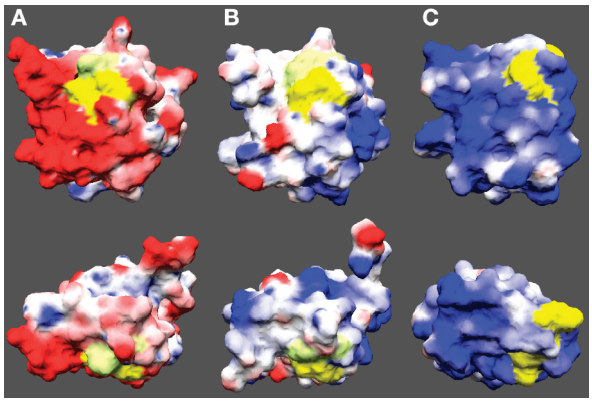

Figure 8. Comparison of molecular surfaces of the three CusF-like proteins or protein domains present in *C. metallidurans* CH34. The molecular surfaces are colored according to the electrostatic potential ranging from −1.8 kT (red) to 1.8 kT (blue). Surfaces of the methionine and tryptophan residues of the metal site are colored yellow and light green, respectively. Molecules are shown in the same orientation as in Figure 7 (top) and after a counterclockwise 90° rotation around the *x*-axis (bottom): (A) *C. metallidurans* $CusB_{425-505}$, (B) *C. metallidurans* $SilB_{440-521}$, and (C) *C. metallidurans* $CusF_{49-123}$.

activated. This is the case for *C. metallidurans* CH34, in which at least three determinants (*cop*, *cus*, and *sil*) are potentially involved in copper resistance.[26,50,69] The *cus* gene cluster present on the bacterial chromosome 2 contains genes encoding a second RND-driven efflux system that potentially regulates copper and silver transport and that contains in particular CusF and CusB proteins. Unlike the corresponding protein in *E. coli*, CusB from *C. metallidurans* CH34 has, like SilB from *C. metallidurans* CH34, a C-terminally fused CusF-like domain. Simultaneous expression of both Sil and Cus systems in *C. metallidurans* CH34 would therefore lead to a situation in which different CusF-like metallochaperones compete for the binding of Cu^+ in the periplasm. Two of these chaperones are fused to the MFP polypeptidic chain of SilB and CusB, whereas CusF is freely diffusing in the periplasm. An important feature of CusF from *C. metallidurans* CH34 is the replacement of the tryptophan residue involved in the coordination site with a methionine. Replacement of the *E. coli* CusF indole side chain with a thioether led to an increase in the Cu^+ affinity by approximately 2 orders of magnitude.[61] This higher substrate affinity of CusF from *C. metallidurans* CH34 would impair the transfer of the metal ions to the efflux complex. This role is probably assumed by the CusF-like domains attached to SilB and CusB from *C. metallidurans* CH34, for which a rapid, intramolecular transfer can occur. It is interesting to note that most organisms that contain CusF-like domains fused to the MFP also contain additional genes encoding CusF-like proteins. In most cases, the metal-binding motif of the fused CusF-like domain is formed by H(X7)W-(X2)MXM, whereas the small, freely diffusing CusF-like proteins contain a H(X7)M(X2)MXM motif or additional, methionine-rich sequences N-terminal to this metal-binding motif that may form other Cu^+-binding sites. This suggests that in these cases, the isolated CusF-like proteins with a higher-affinity metal site may be involved primarily in the sequestration of the metal ions protecting the periplasm from their toxic effects. Exceptions are the *Pseudomonas* species in which the C-terminally fused CusF-like domain contains a H(X7)M-(X2)MXM, whereas the metal sites of the free CusF-like proteins have a tryptophan instead of the first methionine of the metal-binding motif.

The preceding observations, purely based on primary sequence analysis, suggest different specific interactions between numerous mediators involved in heavy metal sequestration and transfer in the periplasm. In the specific case of *C. metallidurans* CH34, we further investigated the different CusF-like metallochaperones by comparing the molecular surface of the experimentally determined $SilB_{440-521}$ structure with those of model structures obtained for $CusB_{425-505}$ and $CusF_{49-123}$ constructed using the I-TASSER server.[70] Figure 8 shows two different views of the molecular surfaces colored according to the electrostatic potential. The three CusF-like domains potentially coexpressed in *C. metallidurans* CH34 differ significantly with respect to their surface potential: whereas $SilB_{440-521}$ appears to be more or less neutral, especially in the proximity of the exposed methionine and tryptophan side chains of the metal-binding site, the two other CusF-like domains are either negatively ($CusB_{425-505}$) or positively ($CusF_{49-123}$) charged. Again this suggests that these CusF-like metallochaperones play different perhaps complementary roles in the sequestration and export of monovalent copper and silver ions.

■ ASSOCIATED CONTENT

Supporting Information. Structure-based multiple-sequence alignment of *C. metallidurans* CH34 MFP (Figure S1), purification of $SilB_{440-521}$ via Tricine-SDS-PAGE and a mass spectrum (Figure S2), comparison of the $^1H,^{15}N$-HSQC spectra of apo- and Ag^+-$SilB_{440-521}$ (Figure S3), assigned $^1H,^{15}N$-HSQC spectrum of apo-$SilB_{440-521}$ (Figure S4), weighted chemical shift differences between apo- and Ag^+-$SilB_{440-521}$ $\{[\Delta HN^2 + \Delta N^2 \times (\gamma_N/\gamma_H)^2]^{1/2}\}$ (Figure S5), and backbone mobility of apo-$SilB_{440-521}$ (Figure S6). This material is available free of charge via the Internet at http://pubs.acs.org.

Accession Codes

Chemical shift assignments and molecular coordinates have been deposited in the BioMagResBank (http://www.bmrb.wisc.edu) as entry 17266 and in the Protein Data Bank (http://www.pdb.org) as entry 2L55, respectively.

■ AUTHOR INFORMATION

Corresponding Author

*Structure and Function of Biological Membranes, Université Libre de Bruxelles, Boulevard du Triomphe CP206/2, 1050 Bruxelles, Belgium. Telephone: (32) 2 650 53 80. Fax: (32) 2 650 53 82. E-mail: vbussche@ulb.ac.be.

Author Contributions

B.B. and K.-M.D. contributed equally to this work.

Funding Sources

This work has been supported by grants from Interuniversity Attraction Poles (IAP) P6/19 (Belgium), the National Fund for Scientific Research (FRFC 2.4527.10 and 2.4533.10), and the SCK·CEN/ULB convention as well as by the Commissariat à l'Energie Atomique, the Centre National de la Recherche Scientifique, and the Université Joseph Fourier. Financial support by the Access to Research Infrastructures activity in the 6th Framework Programme of the EC (Contract RII3-026145, EU-NMR) for conducting the research at the RALF-NMR facility is

gratefully acknowledged, as is support from the Partnership for Structural Biology (PSB, Grenoble, France).

■ ABBREVIATIONS

RND, resistance nodulation cell division; MFP, membrane fusion protein; OMF, outer membrane factor; HAE, hydrophile/amphiphile efflux; HME, heavy metal efflux; MP, membrane proximal.

■ REFERENCES

(1) Zgurskaya, H. I., Yamada, Y., Tikhonova, E. B., Ge, Q., and Krishnamoorthy, G. (2009) Structural and functional diversity of bacterial membrane fusion proteins. *Biochim. Biophys. Acta 1794*, 794–807.

(2) Saier, M. H., Jr., Tam, R., Reizer, A., and Reizer, J. (1994) Two novel families of bacterial membrane proteins concerned with nodulation, cell division and transport. *Mol. Microbiol. 11*, 841–847.

(3) Tseng, T. T., Gratwick, K. S., Kollman, J., Park, D., Nies, D. H., Goffeau, A., and Saier, M. H., Jr. (1999) The RND permease superfamily: An ancient, ubiquitous and diverse family that includes human disease and development proteins. *J. Mol. Microbiol. Biotechnol. 1*, 107–125.

(4) Dong, Q., and Mergeay, M. (1994) Czc/cnr efflux: A three-component chemiosmotic antiport pathway with a 12-transmembrane-helix protein. *Mol. Microbiol. 14*, 185–187.

(5) Nies, D. H., and Silver, S. (1995) Ion efflux systems involved in bacterial metal resistances. *J. Ind. Microbiol. 14*, 186–199.

(6) Nikaido, H., and Takatsuka, Y. (2009) Mechanisms of RND multidrug efflux pumps. *Biochim. Biophys. Acta 1794*, 769–781.

(7) Andersen, C., Hughes, C., and Koronakis, V. (2000) Chunnel vision. Export and efflux through bacterial channel-tunnels. *EMBO Rep. 1*, 313–318.

(8) Fernandez-Recio, J., Walas, F., Federici, L., Venkatesh, P. J., Bavro, V. N., Miguel, R. N., Mizuguchi, K., and Luisi, B. (2004) A model of a transmembrane drug-efflux pump from Gram-negative bacteria. *FEBS Lett. 578*, 5–9.

(9) Lobedanz, S., Bokma, E., Symmons, M. F., Koronakis, E., Hughes, C., and Koronakis, V. (2007) A periplasmic coiled-coil interface underlying TolC recruitment and the assembly of bacterial drug efflux pumps. *Proc. Natl. Acad. Sci. U.S.A. 104*, 4612–4617.

(10) Symmons, M. F., Bokma, E., Koronakis, E., Hughes, C., and Koronakis, V. (2009) The assembled structure of a complete tripartite bacterial multidrug efflux pump. *Proc. Natl. Acad. Sci. U.S.A. 106*, 7173–7178.

(11) Mokhonov, V. V., Mokhonova, E. I., Akama, H., and Nakae, T. (2004) Role of the membrane fusion protein in the assembly of resistance-nodulation-cell division multidrug efflux pump in *Pseudomonas aeruginosa*. *Biochem. Biophys. Res. Commun. 322*, 483–489.

(12) Touze, T., Eswaran, J., Bokma, E., Koronakis, E., Hughes, C., and Koronakis, V. (2004) Interactions underlying assembly of the *Escherichia coli* AcrAB-TolC multidrug efflux system. *Mol. Microbiol. 53*, 697–706.

(13) Tikhonova, E. B., and Zgurskaya, H. I. (2004) AcrA, AcrB, and TolC of *Escherichia coli* form a stable intermembrane multidrug efflux complex. *J. Biol. Chem. 279*, 32116–32124.

(14) Aires, J. R., and Nikaido, H. (2005) Aminoglycosides are captured from both periplasm and cytoplasm by the AcrD multidrug efflux transporter of *Escherichia coli*. *J. Bacteriol. 187*, 1923–1929.

(15) Zgurskaya, H. I., and Nikaido, H. (1999) Bypassing the periplasm: Reconstitution of the AcrAB multidrug efflux pump of *Escherichia coli*. *Proc. Natl. Acad. Sci. U.S.A. 96*, 7190–7195.

(16) Bagai, I., Liu, W., Rensing, C., Blackburn, N. J., and McEvoy, M. M. (2007) Substrate-linked conformational change in the periplasmic component of a Cu(I)/Ag(I) efflux system. *J. Biol. Chem. 282*, 35695–35702.

(17) De Angelis, F., Lee, J. K., O'Connell, J. D., III, Miercke, L. J., Verschueren, K. H., Srinivasan, V., Bauvois, C., Govaerts, C., Robbins, R. A., Ruysschaert, J. M., Stroud, R. M., and Vandenbussche, G. (2010) Metal-induced conformational changes in ZneB suggest an active role of membrane fusion proteins in efflux resistance systems. *Proc. Natl. Acad. Sci. U.S.A. 107*, 11038–11043.

(18) Balakrishnan, L., Hughes, C., and Koronakis, V. (2001) Substrate-triggered recruitment of the TolC channel-tunnel during type I export of hemolysin by *Escherichia coli*. *J. Mol. Biol. 313*, 501–510.

(19) Akama, H., Matsuura, T., Kashiwagi, S., Yoneyama, H., Narita, S., Tsukihara, T., Nakagawa, A., and Nakae, T. (2004) Crystal structure of the membrane fusion protein, MexA, of the multidrug transporter in *Pseudomonas aeruginosa*. *J. Biol. Chem. 279*, 25939–25942.

(20) Higgins, M. K., Bokma, E., Koronakis, E., Hughes, C., and Koronakis, V. (2004) Structure of the periplasmic component of a bacterial drug efflux pump. *Proc. Natl. Acad. Sci. U.S.A. 101*, 9994–9999.

(21) Mikolosko, J., Bobyk, K., Zgurskaya, H. I., and Ghosh, P. (2006) Conformational flexibility in the multidrug efflux system protein AcrA. *Structure 14*, 577–587.

(22) Su, C. C., Yang, F., Long, F., Reyon, D., Routh, M. D., Kuo, D. W., Mokhtari, A. K., Van Ornam, J. D., Rabe, K. L., Hoy, J. A., Lee, Y. J., Rajashankar, K. R., and Yu, E. W. (2009) Crystal structure of the membrane fusion protein CusB from *Escherichia coli*. *J. Mol. Biol. 393*, 342–355.

(23) Mergeay, M., Houba, C., and Gerits, J. (1978) Extrachromosomal inheritance controlling resistance to cadmium, cobalt, copper and zinc ions: Evidence from curing in a *Pseudomonas*. *Arch. Int. Physiol. Biochim. 86*, 440–442.

(24) Mergeay, M., Nies, D., Schlegel, H. G., Gerits, J., Charles, P., and Van Gijsegem, F. (1985) *Alcaligenes eutrophus* CH34 is a facultative chemolithotroph with plasmid-bound resistance to heavy metals. *J. Bacteriol. 162*, 328–334.

(25) von Rozycki, T., and Nies, D. H. (2009) *Cupriavidus metallidurans*: Evolution of a metal-resistant bacterium. *Antonie van Leeuwenhoek 96*, 115–139.

(26) Janssen, P. J., Van Houdt, R., Moors, H., Monsieurs, P., Morin, N., Michaux, A., Benotmane, M. A., Leys, N., Vallaeys, T., Lapidus, A., Monchy, S., Medigue, C., Taghavi, S., McCorkle, S., Dunn, J., van der, L. D., and Mergeay, M. (2010) The complete genome sequence of *Cupriavidus metallidurans* strain CH34, a master survivalist in harsh and anthropogenic environments. *PLoS One 5*, e10433.

(27) Jansson, M., Li, Y. C., Jendeberg, L., Anderson, S., Montelione, B. T., and Nilsson, B. (1996) High-level production of uniformly ^{15}N- and ^{13}C-enriched fusion proteins in *Escherichia coli*. *J. Biomol. NMR 7*, 131–141.

(28) Markley, J. L., Bax, A., Arata, Y., Hilbers, C. W., Kaptein, R., Sykes, B. D., Wright, P. E., and Wuthrich, K. (1998) Recommendations for the presentation of NMR structures of proteins and nucleic acids. IUPAC-IUBMB-IUPAB Inter-Union Task Group on the Standardization of Data Bases of Protein and Nucleic Acid Structures Determined by NMR Spectroscopy. *J. Biomol. NMR 12*, 1–23.

(29) Delaglio, F., Grzesiek, S., Vuister, G. W., Zhu, G., Pfeifer, J., and Bax, A. (1995) NMRPipe: A multidimensional spectral processing system based on UNIX pipes. *J. Biomol. NMR 6*, 277–293.

(30) Johnson, B. A., and Blevins, R. A. (1994) NMR View: A computer program for the visualization and analysis of NMR data. *J. Biomol. NMR 4*, 603–614.

(31) Lescop, E., Schanda, P., and Brutscher, B. (2007) A set of BEST triple-resonance experiments for time-optimized protein resonance assignment. *J. Magn. Reson. 187*, 163–169.

(32) Schanda, P., Van Melckebeke, H., and Brutscher, B. (2006) Speeding up three-dimensional protein NMR experiments to a few minutes. *J. Am. Chem. Soc. 128*, 9042–9043.

(33) Lescop, E., Schanda, P., Rasia, R., and Brutscher, B. (2007) Automated spectral compression for fast multidimensional NMR and increased time resolution in real-time NMR spectroscopy. *J. Am. Chem. Soc. 129*, 2756–2757.

(34) Lescop, E., and Brutscher, B. (2007) Hyperdimensional protein NMR spectroscopy in peptide-sequence space. *J. Am. Chem. Soc. 129*, 11916–11917.

(35) Lescop, E., Rasia, R., and Brutscher, B. (2008) Hadamard amino-acid-type edited NMR experiment for fast protein resonance assignment. *J. Am. Chem. Soc. 130*, 5014–5015.

(36) Lescop, E., and Brutscher, B. (2009) Highly automated protein backbone resonance assignment within a few hours: The "BATCH" strategy and software package. *J. Biomol. NMR 44*, 43–57.

(37) Schanda, P., Kupce, E., and Brutscher, B. (2005) SOFAST-HMQC experiments for recording two-dimensional heteronuclear correlation spectra of proteins within a few seconds. *J. Biomol. NMR 33*, 199–211.

(38) Herrmann, T., Guntert, P., and Wuthrich, K. (2002) Protein NMR structure determination with automated NOE-identification in the NOESY spectra using the new software ATNOS. *J. Biomol. NMR 24*, 171–189.

(39) Herrmann, T., Guntert, P., and Wuthrich, K. (2002) Protein NMR structure determination with automated NOE assignment using the new software CANDID and the torsion angle dynamics algorithm DYANA. *J. Mol. Biol. 319*, 209–227.

(40) Guntert, P., Mumenthaler, C., and Wuthrich, K. (1997) Torsion angle dynamics for NMR structure calculation with the new program DYANA. *J. Mol. Biol. 273*, 283–298.

(41) Cornilescu, G., Delaglio, F., and Bax, A. (1999) Protein backbone angle restraints from searching a database for chemical shift and sequence homology. *J. Biomol. NMR 13*, 289–302.

(42) Brunger, A. T., Adams, P. D., Clore, G. M., DeLano, W. L., Gros, P., Grosse-Kunstleve, R. W., Jiang, J. S., Kuszewski, J., Nilges, M., Pannu, N. S., Read, R. J., Rice, L. M., Simonson, T., and Warren, G. L. (1998) Crystallography & NMR system: A new software suite for macromolecular structure determination. *Acta Crystallogr. DS4*, 905–921.

(43) Farrow, N. A., Muhandiram, R., Singer, A. U., Pascal, S. M., Kay, C. M., Gish, G., Shoelson, S. E., Pawson, T., Forman-Kay, J. D., and Kay, L. E. (1994) Backbone dynamics of a free and phosphopeptide-complexed Src homology 2 domain studied by ^{15}N NMR relaxation. *Biochemistry 33*, 5984–6003.

(44) Dosset, P., Hus, J. C., Blackledge, M., and Marion, D. (2000) Efficient analysis of macromolecular rotational diffusion from heteronuclear relaxation data. *J. Biomol. NMR 16*, 23–28.

(45) Lipari, G., and Szabo, A. (1982) Model-free approach to the interpretation of nuclear magnetic resonance relaxation in macromolecules. 1. Theory and range of validity. *J. Am. Chem. Soc. 104*, 4546–4559.

(46) Lipari, G., and Szabo, A. (1982) Model-free approach to the interpretation of nuclear magnetic resonance relaxation in macromolecules. 2. Analysis of experimental results. *J. Am. Chem. Soc. 104*, 4559–4570.

(47) Poirot, O., Suhre, K., Abergel, C., O'Toole, E., and Notredame, C. (2004) 3DCoffee@igs: A web server for combining sequences and structures into a multiple sequence alignment. *Nucleic Acids Res. 32*, W37–W40.

(48) Rensing, C., Pribyl, T., and Nies, D. H. (1997) New functions for the three subunits of the CzcCBA cation-proton antiporter. *J. Bacteriol. 179*, 6871–6879.

(49) Mergeay, M., Monchy, S., Vallaeys, T., Auquier, V., Benotmane, A., Bertin, P., Taghavi, S., Dunn, J., van der, L. D., and Wattiez, R. (2003) *Ralstonia metallidurans*, a bacterium specifically adapted to toxic metals: Towards a catalogue of metal-responsive genes. *FEMS Microbiol. Rev. 27*, 385–410.

(50) Monchy, S., Benotmane, M. A., Janssen, P., Vallaeys, T., Taghavi, S., van der, L. D., and Mergeay, M. (2007) Plasmids pMOL28 and pMOL30 of *Cupriavidus metallidurans* are specialized in the maximal viable response to heavy metals. *J. Bacteriol. 189*, 7417–7425.

(51) Franke, S., Grass, G., Rensing, C., and Nies, D. H. (2003) Molecular analysis of the copper-transporting efflux system CusCFBA of *Escherichia coli*. *J. Bacteriol. 185*, 3804–3812.

(52) Whittal, R. M., Ball, H. L., Cohen, F. E., Burlingame, A. L., Prusiner, S. B., and Baldwin, M. A. (2000) Copper binding to octarepeat peptides of the prion protein monitored by mass spectrometry. *Protein Sci. 9*, 332–343.

(53) Pelton, J. G., Torchia, D. A., Meadow, N. D., and Roseman, S. (1993) Tautomeric states of the active-site histidines of phosphorylated and unphosphorylated IIIGlc, a signal-transducing protein from *Escherichia coli*, using two-dimensional heteronuclear NMR techniques. *Protein Sci. 2*, 543–558.

(54) Bersch, B., Favier, A., Schanda, P., van Aelst, S., Vallaeys, T., Coves, J., Mergeay, M., and Wattiez, R. (2008) Molecular structure and metal-binding properties of the periplasmic CopK protein expressed in *Cupriavidus metallidurans* CH34 during copper challenge. *J. Mol. Biol. 380*, 386–403.

(55) Sarret, G., Favier, A., Coves, J., Hazemann, J. L., Mergeay, M., and Bersch, B. (2010) CopK from *Cupriavidus metallidurans* CH34 binds Cu(I) in a tetrathioether site: Characterization by X-ray absorption and NMR spectroscopy. *J. Am. Chem. Soc. 132*, 3770–3777.

(56) Murzin, A. G. (1993) OB(oligonucleotide/oligosaccharide binding)-fold: Common structural and functional solution for non-homologous sequences. *EMBO J. 12*, 861–867.

(57) Kim, E. H., Rensing, C., and McEvoy, M. M. (2010) Chaperone-mediated copper handling in the periplasm. *Nat. Prod. Rep. 27*, 711–719.

(58) Loftin, I. R., Franke, S., Roberts, S. A., Weichsel, A., Heroux, A., Montfort, W. R., Rensing, C., and McEvoy, M. M. (2005) A novel copper-binding fold for the periplasmic copper resistance protein CusF. *Biochemistry 44*, 10533–10540.

(59) Guex, N., and Peitsch, M. C. (1997) SWISS-MODEL and the Swiss-PdbViewer: An environment for comparative protein modeling. *Electrophoresis 18*, 2714–2723.

(60) Loftin, I. R., Franke, S., Blackburn, N. J., and McEvoy, M. M. (2007) Unusual Cu(I)/Ag(I) coordination of *Escherichia coli* CusF as revealed by atomic resolution crystallography and X-ray absorption spectroscopy. *Protein Sci. 16*, 2287–2293.

(61) Xue, Y., Davis, A. V., Balakrishnan, G., Stasser, J. P., Staehlin, B. M., Focia, P., Spiro, T. G., Penner-Hahn, J. E., and O'Halloran, T. V. (2008) Cu(I) recognition via cation-π and methionine interactions in CusF. *Nat. Chem. Biol. 4*, 107–109.

(62) Steele, R. A., and Opella, S. J. (1997) Structures of the reduced and mercury-bound forms of MerP, the periplasmic protein from the bacterial mercury detoxification system. *Biochemistry 36*, 6885–6895.

(63) Anastassopoulou, I., Banci, L., Bertini, I., Cantini, F., Katsari, E., and Rosato, A. (2004) Solution structure of the apo and copper(I)-loaded human metallochaperone HAH1. *Biochemistry 43*, 13046–13053.

(64) Rossy, E., Champier, L., Bersch, B., Brutscher, B., Blackledge, M., and Coves, J. (2004) Biophysical characterization of the MerP-like amino-terminal extension of the mercuric reductase from *Ralstonia metallidurans* CH34. *J. Biol. Inorg. Chem. 9*, 49–58.

(65) Chong, L. X., Ash, M. R., Maher, M. J., Hinds, M. G., Xiao, Z., and Wedd, A. G. (2009) Unprecedented binding cooperativity between Cu(I) and Cu(II) in the copper resistance protein CopK from *Cupriavidus metallidurans* CH34: Implications from structural studies by NMR spectroscopy and X-ray crystallography. *J. Am. Chem. Soc. 131*, 3549–3564.

(66) Bagai, I., Rensing, C., Blackburn, N. J., and McEvoy, M. M. (2008) Direct metal transfer between periplasmic proteins identifies a bacterial copper chaperone. *Biochemistry 47*, 11408–11414.

(67) Kittleson, J. T., Loftin, I. R., Hausrath, A. C., Engelhardt, K. P., Rensing, C., and McEvoy, M. M. (2006) Periplasmic metal-resistance protein CusF exhibits high affinity and specificity for both CuI and AgI. *Biochemistry 45*, 11096–11102.

(68) Vaccaro, L., Koronakis, V., and Sansom, M. S. (2006) Flexibility in a drug transport accessory protein: Molecular dynamics simulations of MexA. *Biophys. J. 91*, 558–564.

(69) Monchy, S., Benotmane, M. A., Wattiez, R., van Aelst, S., Auquier, V., Borremans, B., Mergeay, M., Taghavi, S., van der, L. D., and Vallaeys, T. (2006) Transcriptomic and proteomic analyses of the pMOL30-encoded copper resistance in *Cupriavidus metallidurans* strain CH34. *Microbiology 152*, 1765–1776.

(70) Zhang, Y. (2008) I-TASSER server for protein 3D structure prediction. *BMC Bioinf. 9*, 40.